Heliyon 10 (2024) e23913

Contents lists available at ScienceDirect

Heliyon

journal homepage: www.cell.com/heliyon

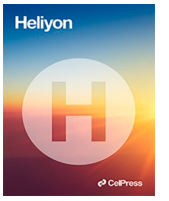

Proteomic analysis reveals LRPAP1 as a key player in the micropapillary pattern metastasis of lung adenocarcinoma

Hao-jie Yan [a,b,c,1], Sheng-cheng Lin [e,1], Shao-hang Xu [f], Yu-biao Gao [a,c], Bao-jin Zhou [g], Ruo Zhou [f], Fu-ming Chen [a,c], Fu-rong Li [a,c,d,*]

[a] *Translational Medicine Collaborative Innovation Center, Shenzhen People's Hospital (The Second Clinical Medical College, Jinan University, The First Affiliated Hospital, Southern University of Science and Technology), 518020, Shenzhen, China*
[b] *Post-doctoral Scientific Research Station of Basic Medicine, Jinan University, 510632, Guangzhou, China*
[c] *Guangdong Engineering Technology Research Center of Stem Cell and Cell Therapy, Shenzhen Key Laboratory of Stem Cell Research and Clinical Transformation, Shenzhen Immune Cell Therapy Public Service Platform, 518020, Shenzhen, China*
[d] *Institute of Health Medicine, Southern University of Science and Technology, 518055, Shenzhen, China*
[e] *Department of Thoracic Surgery, National Cancer Center/National Clinical Research Center for Cancer/Cancer Hospital and Shenzhen Hospital, Chinese Academy of Medical Sciences and Peking Union Medical College, 518172, Shenzhen, China*
[f] *Deepxomics Co., Ltd, 518112, Shenzhen, China*
[g] *Experiment Center for Science and Technology, Shanghai University of Traditional Chinese Medicine, 201203, Shanghai, China*

A R T I C L E I N F O

Keywords:
Lung adenocarcinomas
Micropapillary
Metastasis
LRPAP1
Proteomics

A B S T R A C T

Objectives: Lung adenocarcinomas have different prognoses depending on their histological growth patterns. Micropapillary growth within lung adenocarcinoma, particularly metastasis, is related to dismal prognostic outcome. Metastasis accounts for a major factor leading to mortality among lung cancer patients. Understanding the mechanisms underlying early stage metastasis can help develop novel treatments for improving patient survival.

Methods: Here, quantitative mass spectrometry was conducted for comparing protein expression profiles among various histological subtypes, including adenocarcinoma in situ, minimally invasive adenocarcinoma, and invasive adenocarcinoma (including acinar and micropapillary [MIP] types). To determine the mechanism of MIP-associated metastasis, we identified a protein that was highly expressed in MIP. The expression of the selected highly expressed MIP protein was verified via immunohistochemical (IHC) analysis and its function was validated by an in *vitro* migration assay.

Results: Proteomic data revealed that low-density lipoprotein receptor-related protein–associated protein 1 (LRPAP1) was highly expressed in MIP group, which was confirmed by IHC. The co-expressed proteins in this study, PSMD1 and HSP90AB1, have been reported to be highly expressed in different cancers and play an essential role in metastasis. We observed that LRPAP1 promoted lung cancer progression, including metastasis, invasion and proliferation *in vitro* and *in vivo*.

Conclusion: LRPAP1 is necessary for MIP-associated metastasis and is the candidate novel anti-metastasis therapeutic target.

* Corresponding author. Translational Medicine Collaborative Innovation Center, Shenzhen People's Hospital (The Second Clinical Medical College, Jinan University, The First Affiliated Hospital, Southern University of Science and Technology), 518020, Shenzhen, China.
E-mail address: lifurong@mail.sustech.edu.cn (F.-r. Li).
[1] These authors contributed equally to this work.

https://doi.org/10.1016/j.heliyon.2023.e23913
Received 4 August 2023; Received in revised form 13 December 2023; Accepted 15 December 2023
Available online 20 December 2023
2405-8440/© 2023 The Authors. Published by Elsevier Ltd. This is an open access article under the CC BY-NC-ND license (http://creativecommons.org/licenses/by-nc-nd/4.0/).

1. Introduction

Lung adenocarcinoma (LUAD) shows the highest prevalence among lung cancer subtypes, and it accounts for a main cause of cancer-related death worldwide [1]. Regardless of advances in clinical technology, lung cancer patients still have a low (22 %) 5-year relative survival rate [1]. Metastasis represents a leading factor inducing mortality among cancer patients [2]. A LUAD classification system has been proposed by International Association for the Study of Lung Cancer, American Thoracic Society, and European Respiratory Society. It divides LUAD into pre-invasive subtype (like atypical adenomatous hyperplasia [AAH], adenocarcinoma in situ [AIS], and minimally invasive adenocarcinoma [MIA]) or invasive adenocarcinoma (IAC) (namely, lepidic [LEP], acinar [ACI], papillary [PAP], micropapillary [MIP], or solid [SOL] predominant subtype) [3].

Abbreviations

AIS	adenocarcinoma in situ
MIA	minimally invasive adenocarcinoma
IAC	invasive adenocarcinoma
ACI	acinar
MIP	micropapillary
IHC	immunohistochemistry
LRPAP1	ipoprotein receptor-related protein–associated protein 1
PSMD1	pteasome 26 S subunit, non-ATPase 1
HSP90AB1	heat shock protein 90 alpha family class B member 1
LUAD	lung adenocarcinoma
AAH	atypical adenomatous hyperplasia
LEP	lepidic
PAP	papillary
SOL	solid
LRP1	low-density lipoprotein receptor-related protein 1
BCR	B-cell receptors
MCL	mantle cell lymphoma
ESCC	esophageal squamous cell carcinoma
FFPE	frmalin-fixed, paraffin-embedded
BCA	bicinchoninic acid
FASP	filter-aided sample preparation
GO	Gene Ontology
KEGG	Kyoto Encyclopedia of Genes and Genomes
STR	short tandem repeat
qRT-PCR	quantitative reverse transcription-polymerase chain reaction
FBS	fetal bovine serum
MTS	3-(4,5-dimethylthiazol-2yl)-5- (3-carboxymethoxyphenyl)-2-(4-sulfophenyl)-2H-tetrazolium
DFS	disease-free survival
RFP	recurrence-free probability
HPA	Human Protein Atlas
TAM	tumor-associated macrophage
CPTAC	Clinical Proteomic Tumor Analysis Consortium
PCN	protein co-expression network
LDCT	low-dose computed tomography
IASLC	International Association for the Study of Lung Cancer
ATS	American Thoracic Society
ERS	European Respiratory Society

Surgical resection is highly effective for pre-invasive lesions, with a 5-year survival rate of about 100 %. However, IAC has a much lower survival rate, which decreases substantially with increasing tumor stage [4]. LEP- and ACI-predominant subtypes of IAC are less invasive and have a better prognosis than the other histological subtypes [5–9]. In contrast, PAP-predominant LUAD generally exhibits an intermediate prognosis [10,11]. MIP- and SOL-predominant subtypes of IAC exhibit the poorest prognosis. With regard to MIP-predominant LUAD, its 5-year disease-free survival (DFS) rate is 0 % [12], and overall survival (OS) is markedly dismal within tumors with even 1 % MIP pattern [13]. Recent studies have used genome sequencing to generate genetic maps of different histological subtypes in all-stage tumor tissues [14,15]. However, the mechanism of MIP-associated metastasis remains unknown and studies at a similar proteomic level are lacking.

Low-density lipoprotein receptor-related protein-associated protein 1 (LRPAP1) served as the chaperone for low-density

lipoprotein receptor-related protein 1 (LRP1). It regulates apoE-enriched lipoprotein absorption and activates α2-macroglobulin within extra- and intra-hepatic tissues [16,17]. LRPAP1 loss leads to LRP1 deficiency, which may result in transforming growth factor-β signaling activation and abnormal extracellular matrix (ECM) remodeling, eventually leading to myopia [18,19]. LRPAP1 was recently identified as an autoantigen for B-cell receptors (BCR) from mantle cell lymphoma (MCL) that induces proliferation via the BCR pathway [20]. LRPAP1 autoantibodies are related to superior outcomes among MCL patients [21]. In contrast, LRPAP1 is overexpressed in esophageal squamous cell carcinoma, and its serum antibody is a valuable marker for diagnosing digestive organ cancers and atherosclerosis-related diseases [22]. Nonetheless, roles of LRPAP1 within lung cancer and metastasis remain largely unclear.

To delineate the unique molecular features of different LUAD histological subtypes, quantitative mass spectrometry (MS) was applied in comparing following four groups of tumor tissues at pathological stage I with no metastasis: AIS, MIA, ACI, and MIP. Bioinformatics analyses revealed that LRPAP1 expression gradually increased from AIS to MIA, ACI, and MIP. LRPAP1 was also co-expressed with many proteins linked to cancer metastasis, such as PSMD1 and HSP90AB1. *In vitro* cell migration assays revealed that LRPAP1 overexpression promoted cancer cell metastasis and invasion. Here, we conducted a comprehensive proteomic analysis of different LUAD histological subtypes to identify the cause of MIP-associated metastasis and emphasize the feasibility of LRPAP1 as the target for anti-metastatic treatment.

2. Materials and methods

2.1. Human samples

Formalin-fixed paraffin-embedded (FFPE) samples (n = 24) were obtained from Cancer Hospital (Shenzhen), Chinese Academy of Medical Sciences, and Peking Union Medical College. The basic and clinical patient features can be observed from Table 1.

2.2. Ethical approval

The present work gained approval from Cancer Hospital and Shenzhen Hospital, Chinese Academy of Medical Sciences, and Peking Union Medical College Institutional Review Board of Clinical Research (ethics approval reference no. KYKT2021-2-1). Patients provided informed consents for participation.

2.3. Protein extraction and digestion

Proteins were extracted from FFPE samples as previously described [23]. We utilized the bicinchoninic acid protein assay kit (Beyotime Institute of Biotechnology, China) in assessing protein content within lysate.

Meanwhile, proteins were digested by filter-aided sample preparation method described previously [24]. Briefly, proteins were extracted within the ultrafiltration filtrate tube (30 kDa cut-off, Sartorius, Germany), then UA buffer (100 μL, comprising 8 M urea, 10 mM IAM, and 150 mM Tris-HCl, pH 8.0) was introduced to conduct 30-min incubation. Samples were rinsed twice using UB buffer (100 μL, consisting of 8 M urea, and 150 mM Tris-HCl, pH 8.0) in the filter unit. After 10-min centrifugation at 12,000 g, 100 μL ABC and trypsin (Promega, USA) were added to digest protein suspension within this infiltrate tube for an 18-h period at 37 °C. Finally, liquid chromatography (LC)-MS analysis was performed on the filtrate that was centrifuged for a 10-min period at 12,000 g.

Table 1
Clinicopathological characteristics of different lung adenocarcinoma histologic subtypes.

Characteristic	Total	AIS	MIA	ACI	MIP	*p-value*
	(n = 24)	(N = 7 [29 %])	(N = 7 [29 %])	(N = 6 [25 %])	(N = 4 [17 %])	
Age (years)	60 (32–78)	60 (32–69)	60 (33–70)	62.5 35–78)	67 (43–71)	0.78
Smoking status						0.804
Never	9 (38)	2 (29)	3 (43)	3 (50)	1 (25)	
Ever	15 (62)	5 (71)	4 (57)	3 (50)	3 (75)	
cN status						0.801
Node-negative	24 (100)	7 (100)	7 (100)	6 (100)	4 (100)	
Node-positive	0 (0)	0 (0)	0 (0)	0 (0)	0 (0)	
pN status						0.157
Node-negative	23 (96)	7 (100)	7 (100)	6 (100)	3 (75)	
Node- positive	1 (4)	0 (0)	0 (0)	0 (0)	1 (25)	
VPI	3 (13)	0 (0)	0 (0)	1 (17)	2 (50)	0.0647
LVI	3 (13)	0 (0)	0 (0)	0 (0)	3 (75)	<0.001

Data are no. (%), or median. cN status, clinical node status; pN status, pathological node status; VPI, visceral pleural invasion; LVI, lymphovascular invasion. Continuous variables (age) were analyzed using analysis of variance (ANOVA). Discrete variables (such as pN. status) were analyzed by chi-square test.

2.4. LC-MS/MS analysis

The EASY-nano-LC 1000 system (Thermo Fisher Scientific, MA, USA) was used for separating peptides, which were later emitted in Q-Exactive HF tandem mass spectrometer (Thermo Fisher Scientific) by the Acclaim PepMap C18 column (3 μm, 100 Å, 75 μm × 50 cm, Thermo Fisher Scientific). Solvent A included 0.1 % formic acid supplemented within water, whereas solvent B was comprised by 0.1 % formic acid contained within 98 % acetonitrile. The injection volume was 3 μL (about 3 μg) each time, and the elution procedure (60-min) was as follows, 5-min at 5 % B, 10-min at 20 % B, 10-min at 32 % B, and 10-min at 90 % B. At last, B was reduced to 5 % within the following 60 s, followed by 10-min equilibration prior to subsequent injection.

A Thermo Q-Exactive HF mass spectrometer was programmed for obtaining 55 × 16 *m/z* spectra (16 *m/z* precursor isolation windows, resolution of 30,000, AGC target of 1e5, and maximal injection time of 55 ms) in data independent acquisition (DIA) mode for quantitative samples. We obtained precursor spectra (350–1500 *m/z*) at a 120,000 resolution for hitting the AGC target of 3e6. The maximal injection time was 50 ms.

2.5. Protein identification

The library-free method [25] was applied in analyzing DIA data using DIA-NN algorithm. To generate the library, the options "Deep learning-based spectra, RTs, and IMs prediction" and "FASTA digest for library-free search/library generation" were enabled. Operating in this mode, DIA-NN first generates an in silico-predicted spectral library from a human protein sequence database (UniProt version 2018.7, comprising 20,386 entries). DIA-NN subsequently analyzes the raw data employing this library. Match between runs (MBR) was also activated. The following parameters were employed for the database search: enzyme, trypsin/P; maximal missed cleavages, 2; fixed modification, carbamidomethyl (C); variable modifications, oxidation (M). The 1 % false discovery rate was applied in filtering results. Just protein groups passing the standard could be adopted for downstream analyses.

2.6. Bioinformatic data analysis

R statistical environment software (version 4.2.0; R Foundation for Statistical Computing, Vienna, Austria) was applied in statistical analysis. Complex Heatmap package (version 2.8.0) was adopted for generating the hierarchical clustering heatmap. Next, hypergeometric-based enrichment analysis was performed for each group using several annotation systems, including Gene Ontology, Kyoto Encyclopedia of Genes and Genomes, EggNOG, and Reactome systerms. Finally, the co-expressed proteins were imported into Cytoscape to construct a network.

2.7. Cell culture and reagents

We obtained A549 and H1975 cells in Cell Bank of Shanghai Institutes for Biological Sciences of the Chinese Academy of Sciences (Shanghai, China). To ensure cell line quality, we identified short tandem repeat and detected mycoplasma. Cells were grown within the Dulbecco's modified Eagle's medium (DMEM, Thermo Fisher Scientific) that included 10 % fetal bovine serum (FBS, Thermo Fisher Scientific) under 37 °C and 5 % CO_2, maintaining a pH level of around 7.2–7.6. The medium was refreshed at 2–3-day intervals, and cells were passaged every 2–3 days when coverage reached 80–90 %.

2.8. Quantitative reverse transcription-polymerase chain reaction (qRT-PCR)

The TRIzol reagent (Thermo Fisher Scientific) was utilized for extracting total cellular RNA following specific instructions. Later, total RNA (1 μg) was prepared to cDNA with PrimerScript RT reagent kit (Takara, Kyoto, Japan). qRT-PCR analysis was conducted by SYBR Green Master Mix (Takara). Glyceraldehyde 3-phosphate dehydrogenase (GAPDH) served as the endogenous reference. qRT-PCR primers below were used: *GAPDH*, ACGGATTTGGTCGTATTGGG (forward) and CGCTCCTGGAAGATGGTGAT (reverse); *LRPAP1*, ACCTCAATGTCATCTTGG (forward) and CTTTGTGATGCAGGAACTC (reverse).

2.9. Western blotting

We conducted Western-blotting according to previous description [26]. *Anti*-LRPAP1 (1:1000; Abcam, MA, USA) and *anti*-GAPDH (1:1000; Abcam) primary antibodies and a secondary antibody against rabbit immunoglobulin G (1:1000, Cell Signaling Technology, MA, USA) were used. Enhanced chemiluminescence (Millipore, Burlington, MA, USA) was later adopted for detecting protein expression.

2.10. Lentivirus infection

The overexpression and knockdown lentivirus were provided by GeneChem (Shanghai, China). In brief, 5×10^5 cells were inoculated in a six-well plate for 24-h incubation till reaching 80 % confluency. The lentiviruses were mixed with the transfection reagent, in line with specific instructions. At 72-h following virus application, 1 μg/mL puromycin was used for screening stably infected cells. qRT-PCR and Western-blotting were carried out to confirm infection efficiency.

2.11. Transwell assay

Lower chamber of Transwell plate was introduced with medium (600 μL) that contained 20 % FBS. Then, top chamber was introduced with 200 μL FBS-free cell suspension that contained 1×10^5 cells. Following 24-h incubation, a cotton swab was utilized to remove remaining cells from the inner chamber membrane. While cells migrating onto outer chamber membrane were stained using 0.5 % crystal violet. After 30-min drying under 80 °C, images of at least five random fields were taken using an inverted microscope. The cells were quantified using Image J software. Specifically, we chose three images for each group, converted the image to black and white and adjusted the threshold to contain all cells as much as possible while removing impurities in the background. ImageJ enabled reliable automated cell counting following 'Analyze Particles', as well as manual confirmation of accuracy.

2.12. Wound healing assay

About 1×10^6 cells/well were inoculated in the 6-well plate and allowed for overnight formation of monolayers. A straight line was created with a sterilized 20-μL pipette tip across surface of the plates, and phosphate-buffered saline was used thrice to remove the suspended cells. Images of control group were obtained at 0 h. Then, 24-h cell culture in DMEM including 2 % FBS under 37 °C with 5 % CO2 was completed. Finally, mages were captured using a phase-contrast microscope. Each assay was performed in triplicates. The scratch areas were quantified using ImageJ software. Briefly, we first calculated the scratch area at day 0 denoted by S0, then calculated the area S1 after 24 h, and finally, used (S0–S1)/S0 to calculate the migration efficiency.

2.13. Flow cytometry analysis and apoptosis assay

Flow cytometry analysis was performed using the FC500-MPL flow cytometer (Beckman Coulter), as previously described [27]. Apoptosis assays were performed using the YF®647A-Annexin V and PI Apoptosis Kits (UE, Suzhou, China). Data were analyzed using the FlowJo software.

2.14. 3-(4,5-dimethylthiazol-2yl)-5-(3-carboxymethoxyphenyl)-2-(4-sulfophenyl)-2H-tetrazolium (MTS) assay

Using MTS cell proliferation and cytotoxicity assay kit (KeyGen, Nanjing, China), cell proliferation was measured within the 96-well plate (1000 cells/well) in line with specific protocols.

2.15. Immunohistochemical (IHC) analysis

IHC was carried out using FFPE sections stained with LRPAP1 (Abcam), as previously described [28]. Finally, sections were viewed and photographed in at least five random fields using a confocal microscope (Leica, Germany). Immunoreactivity was assessed using the previously described immunoreactivity score (IRS) method [29]. Briefly, IRS = staining intensity (SI) × positive percentage (PP). The SI is categorized into four levels: 0 (negative), 1 (weak), 2 (moderate), and 3 (strong). The PP is classified into five levels: 0 (negative, ≤10 %), 1 (11%–25 %), 2 (26%–50 %), 3 (51%–75 %), and 4 (76%–100 %).

2.16. Animal experiments

The 5-6-week-old female BALB/c mice were provided by GemPharmatech (Jiangsu, China) and raised under the specific pathogen-free (SPF) condition. Mice were given subcutaneous injection with a suspension containing 5×10^6 cells within PBS-matrigel (200 μL; ratio, 1:1). Tumor formation was monitored post-injection, and the weight of mice with tumor volumes was measured twice a week.

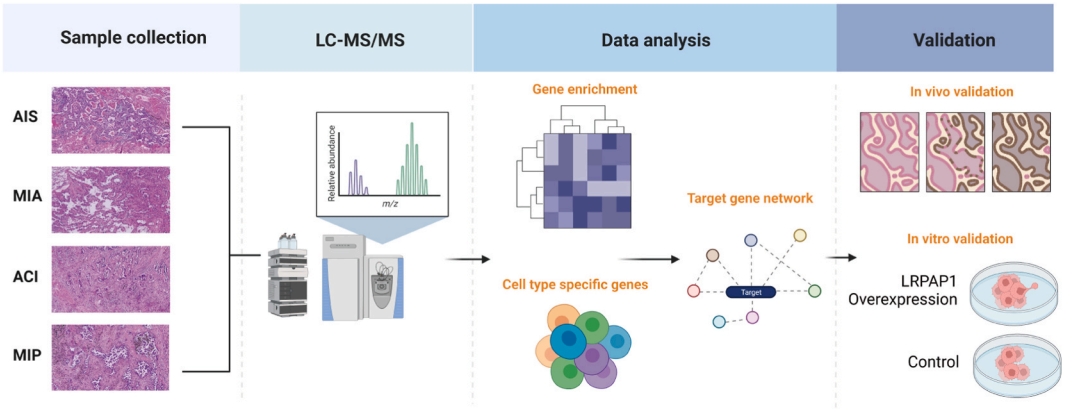

Fig. 1. Study design for the proteome analysis of different lung adenocarcinoma histologic subtypes. The flowchart was created on BioRender.com.

3. Results

3.1. Study design focused on different LUAD histologic subtypes

We collected FFPE tissue samples from seven AIS, seven MIA, six ACI, and four MIP lung tumors for this study. Table 1 displays basic patient features. All samples were classified as pathological stage I. ACI and MIP accounted for >40 % of the corresponding samples.

Quantitative proteomic data were acquired for different histological subtypes of LUAD. There were altogether 6022 unique proteins discovered and analyzed using a label-free DIA MS workflow (Table S1). We conducted extensive bioinformatics analyses and

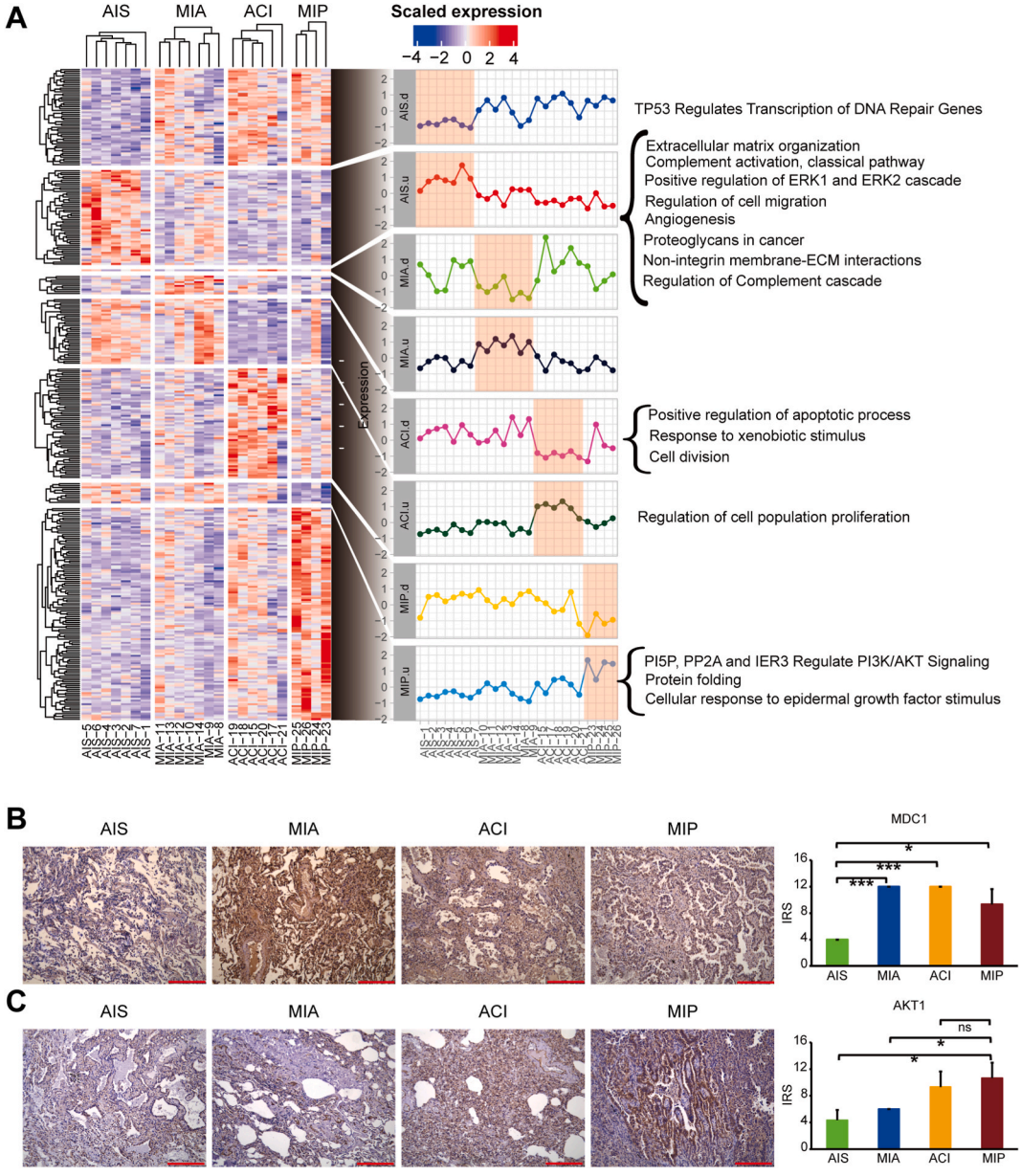

Fig. 2. Heat map of gene enrichment analysis. (A) Significantly altered proteins were classified into eight clusters (right panel). Normalized abundance in each row was calculated using the Z-score method. Temporal patterns (middle panel) were used to visualize the relevant changes in each cluster. The core functional entries were labeled in the right panel of the figure after a manual review. u, up; d, down. (B–C) Representative immunostaining images and corresponding statistical comparison histograms (right) for MDC1 (B) and AKT1 (C) in the tumor tissues from each group. Scale bars, 250 μm. Data were presented as mean ± SD. Statistical significance between groups was determined using Kruskal-Wallis nonparametric analysis. *P < 0.05; ***P < 0.001; ns, not significant.

validated potential proteins related to tumor metastasis *in vivo* and *in vitro* (the study design is shown in Fig. 1). Mass spectrometry proteomics data were imported in ProteomeXchange Consortium (http://proteomecentral.proteomexchange.org) through iProX partner repository [30,31] under the dataset identifier PXD038594.

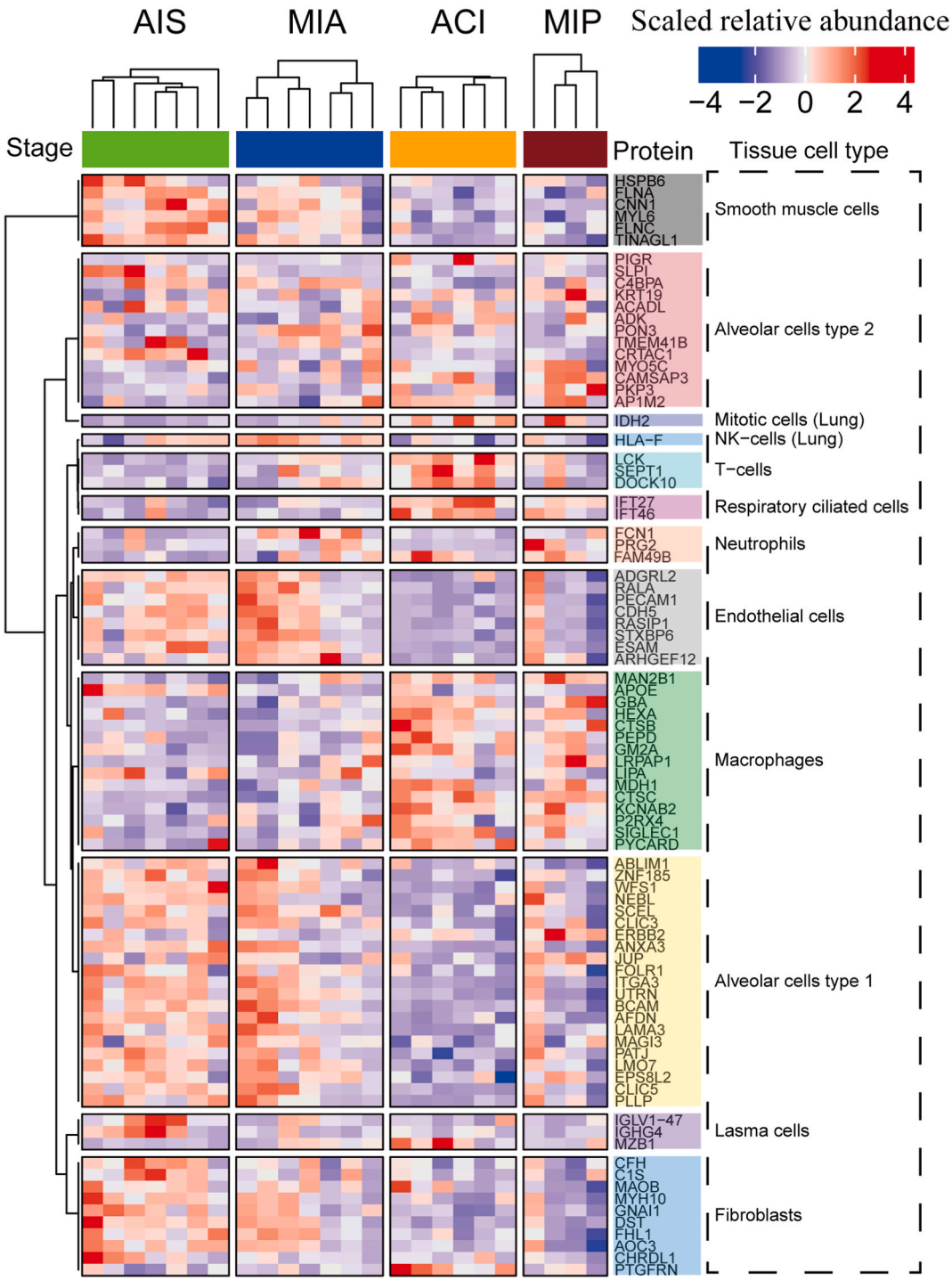

Fig. 3. Lung cell type-specific enrichment analysis. Significantly altered proteins were subdivided into 12 categories. Z-score approach was applied in calculating normalized abundances of diverse rows. Tissue cell type column indicates the cell types in each cluster, and the protein column indicates the identified protein for the corresponding cell types.

3.2. Proteins and pathways associated with different LUAD histologic subtypes

All samples from different subtypes had similar protein numbers and total protein intensity distributions (Figs. S1A–B). In addition, quantitative reproducibility was satisfactory for further statistical analyses (Fig. S1C).

Based on the quantified proteins, we identified different genes (Table S2, Fig. S2) and pathways enriched in the different subtypes (Fig. 2A). We also found that the TP53-regulated transcription of DNA repair proteins was downregulated in the AIS group, consistent with the onset of cancer (Fig. 2A). Moreover, the expression of MDC1, a representative protein in this pathway, was corroborated by IHC analysis (Fig. 2B). Defects in DNA repair and damage signaling contribute to tumorigenesis [32–34]. TP53 is a well-known tumor suppressor that encodes a transcription factor that regulates downstream antitumor responses such as DNA repair and apoptosis [35]. More than 50 % of cancers have abnormal TP53 function [36,37]. Proteins enriched in the AIS group were primarily associated with pulmonary physiological function (pulmonary immunity and ventilation)-related pathways [38,39], including ECM organization and complement cascade regulation (Fig. 2A). AIS and MIA tumors are defined as lesions $\leq$3 cm in size. Multiple validation studies have shown that both tumors show a 100 % 5-year DFS (disease-free survival) rate after complete resection. The lung in AIS and MIA tumors are primarily functional, with only minor damage. These results indicated that our proteomic data were highly reliable.

Prognosis of ACI-predominant LUAD is worse than that of AIS and MIA, with the 70–80 % 5-year relapse-free probability [9]. Here, highly expressed proteins in the ACI group were associated with cell proliferation. In contrast, pathways related to apoptosis and cell division were downregulated (Fig. 2A). This finding may explain why ACI-dominated tumors show an increased relapse risk than AIS or MIA tumors.

MIP growth in LUAD is associated with lymphatic and pleural invasion, nodal metastases, and a 5-year DFS rate of 0 %. Minor MIP patterns can lead to adverse clinical outcomes [12]. OS is significantly worse in tumors with even 1 % MIP patterns [13]. However, the mechanisms underlying MIP-associated invasion and metastasis is unknown. According to our results, PI3K/AKT pathway was upregulated within MIP tumors (Fig. 2A), which was associated with cancer onset and development and played key roles in tumor cell proliferation, migration, and metabolism [40–42]. Furthermore, the expression of AKT1, a key protein in this pathway, was validated by IHC analysis (Fig. 2C). This could partly explain why MIP tumors are prone to metastasis and recurrence.

3.3. Macrophages are highly enriched in MIP based on cell type analysis

Heterogeneity is characteristic of many biological systems and diseases, including cancer [43,44]. For example, tumor cell type analysis, such as single-cell RNA-sequencing, contributes to revealing uncommon and complicated cell subsets and gene regulatory relations and tracking development trajectory in diverse cells [45]. To investigate cell types of the identified proteins, we used lung cell-type specificity annotation from the tissue cell-type section in Human Protein Atlas (www.proteinatlas.org/) database [46]. We found that smooth muscle cells and fibroblasts, which form and maintain typical tissue structure [47], were enriched in AIS (Fig. 3). In contrast, these cell types were gradually decreased in MIA, ACI, and MIP groups (Fig. S3). Our data provide an accurate picture of what happens in the lungs as prognosis worsens from AIS to MIA, ACI, and MIP. Mitotic and T cells were enriched in the ACI group, indicating that tumor cell proliferation and antitumor immunity occur concurrently (Fig. 3). These findings support the assertion that ACI has an intermediate prognosis [4]. Macrophages were enriched in ACI and MIP groups (Fig. 3). Macrophages play essential roles in cancer development and metastasis [48]. Anti-inflammatory and tumor-associated M2 macrophages enhance tumor proliferation and migration [49].

3.4. LRPAP1 is highly-expressed in MIP via IHC validation

Macrophages were enriched in the ACI and MIP groups. Among the 15 proteins in the macrophage set (Fig. 3), only LRPAP1 of MIP group was up-regulated relative to those remaining three groups (Table S2). IHC analysis was used to confirm the expression pattern in our proteomic data by verifying the expression of LRPAP1 in the four groups. LRPAP1 was highly expressed in MIP (Fig. 4).

3.5. LRPAP1 and its co-expressed proteins are all highly expressed in tumors

LRPAP1 was first identified as an LRP1 chaperone that modulates ApoE-enriched lipoprotein uptake and activates α2-macroglobulin within extra- and intra-hepatic tissues [16,17]. It is important for occurrence of myopia and MCL [18–21]. But its impact on solid tumors remains ambiguous. To investigate the role of LRPAP1 in solid tumors, we identified a network of proteins that were

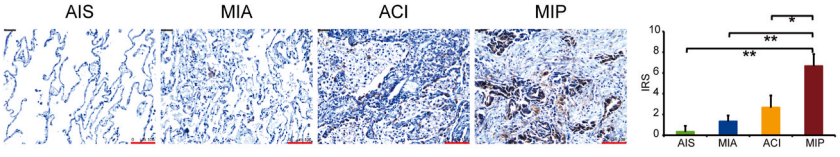

Fig. 4. Low-density lipoprotein receptor-related protein-associated protein 1 (LRPAP1) highly expressed in micropapillary (MIP) adenocarcinoma. Representative immunostaining images and corresponding statistical comparison histograms (right) for LRPAP1 in the tumor tissues from each group. Scale bars = 100 μm. Data were presented as mean ± SD. Statistical significance between groups was determined using Kruskal-Wallis nonparametric analysis. *P < 0.05, **P < 0.01.

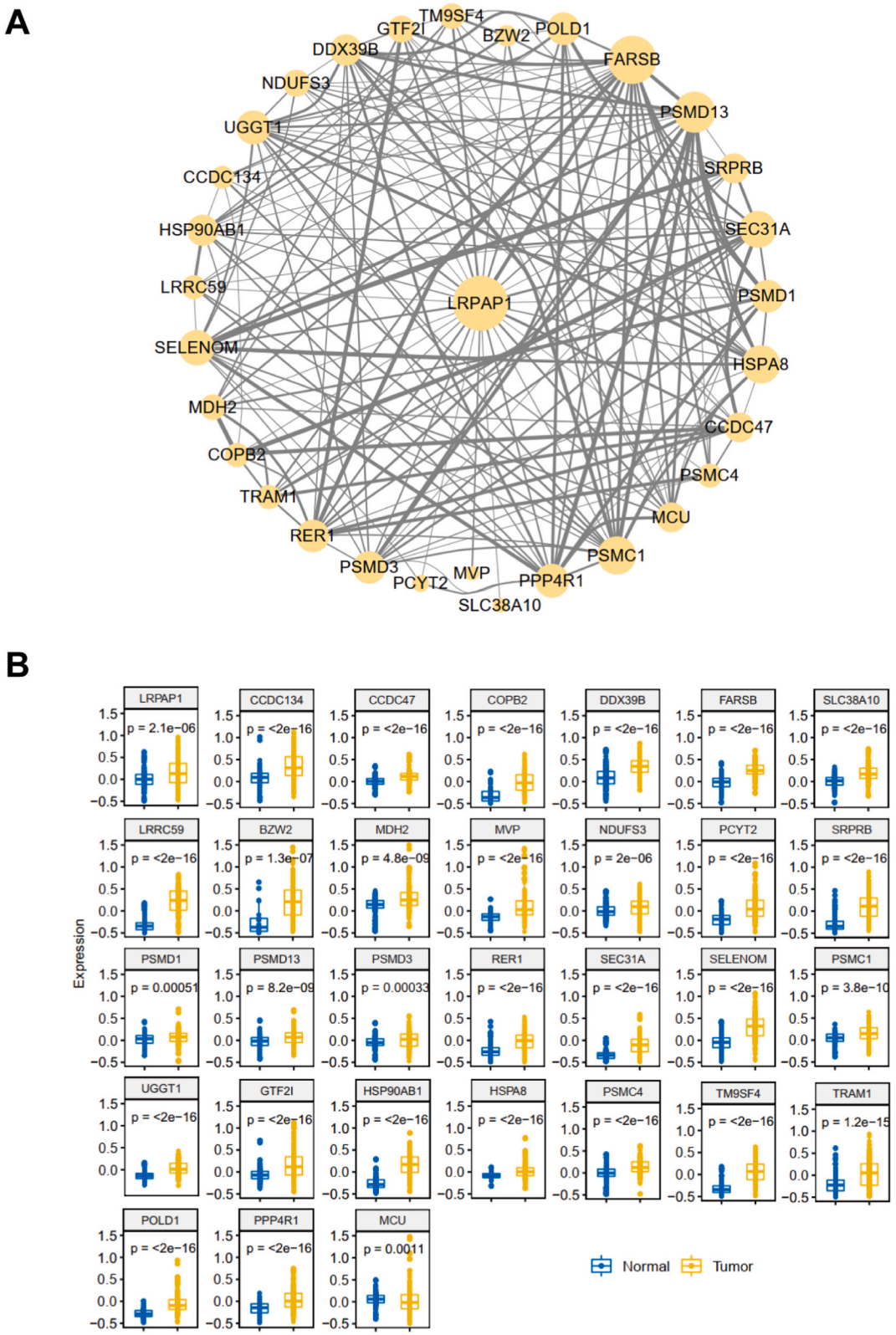

Fig. 5. Protein co-expression network (PCN) of LRPAP1. (A) All proteins with a Pearson's correlation >0.8 with LRPAP1 were defined as co-expressed proteins and illustrated as a network. The node indicates a protein, and the edge indicates the corresponding correlation value

between proteins. (B) Abundance comparison of co-expressed proteins in lung cancer data from Clinical Proteomic Tumor Analysis Consortium (CPTAC).

highly co-expressed with LRPAP1 in LUAD (Fig. 5A). According to Clinical Proteomic Tumor Analysis Consortium (CPTAC) database, 30 proteins were co-expressed with LRPAP1, all of which were highly expressed in tumors relative to paracancerous tissues (Fig. 5B). This dataset is freely accessible [50]. Therefore, LRPAP1 is crucial for tumor development. However, further investigation is necessary for illustrating molecular mechanisms of LRPAP1 in enhancing tumor growth and metastasis.

3.6. LRPAP1 promotes metastasis of cancer cells

Metastasis accounts for a major factor inducing mortality among lung cancer patients [2]. MIP-predominant IAC subtype has the poorest prognosis among all subtypes and is associated with metastasis [12]. MIP subtype is highly migratory, with no method to inhibit its metastasis. Here, as suggested by our proteomic data, LRPAP1 showed high expression within MIP. Therefore, we overexpressed LRPAP1 in A549 and H1975 lung cancer cells (Figs. S4A–B), to investigate its potential role in cancer cell metastasis. We performed transwell and wound healing assays to examine cell migration and invasion. LRPAP1-overexpressing cells had significantly higher migratory capacity than the control cells in both A549 and H1975 cells lines (Fig. 6A and B). Furthermore, we measured cell growth and viability to rule out possible confounding impacts of LRPAP1 overexpression on cell growth and death. As shown in Figs. S4C–D, increased LRPAP1 expression did not affect the apoptosis but slightly increased the proliferation of cells after 72 h. To further elucidate the role of LRPAP1 in tumor development, we knocked down LRPAP1 (LRPAP1-KD, Figs. S4E–F). This resulted in a significant inhibition of cell migration and invasion compared to the control group (Fig. 6C and D). Given the compelling *in vitro* findings, we sought to validate LRPAP1's impact *in vivo*. Equal numbers of cells overexpressing LRPAP1 or control cells were separately injected subcutaneously into BALB/c nude mice. The results demonstrated that LRPAP1 overexpression promoted tumor growth (Fig. 6E). Tumor volumes and weights were significantly larger in the group with overexpressed LRPAP1 compared to the control group (Fig. 6F–H). Notably, there was no significant difference in mouse weight between the two groups throughout the tumor-bearing process (Figs. S4G–H).

4. Discussion

Lung cancer accounts for a main factor resulting in cancer-associated mortality globally [1]. Lung cancer metastasis represents an important cause of cancer-related deaths [2]. Low-dose computed tomography (LDCT) helps decrease the lung cancer-specific death rate by 20 % [51]. But, lung cancer detection is inadequate, with no effective treatment for metastatic or potentially metastatic lung cancer. LUAD, a lung cancer histological subtype with the highest prevalence, has a poor prognosis and occupies 40 % of the entire lung cancer patients [52]. LUAD includes many histological subtypes, among which the 5-year DFS for MIP-predominant LUAD is 0 % [12] and the OS is significantly worse in tumors with even 1 % MIP pattern [13]. However, the mechanisms underlying MIP-associated metastasis remain unclear.

Recent studies have used genome sequencing to generate genetic maps of different histological subtypes of lung cancer at all stages [14,15]. However, no protocol is currently available for the inhibition of MIP-mediated metastasis. Therefore, we performed proteomic analyses of AIS-, MIA-, ACI-, and MIP-predominant tumors in Phase I. We chose the Phase I samples for two main reasons. First, the Phase I sample population was significant, taking up 80 % of the entire lung cancer patients. Second, studying metastasis in early samples in conjunction with LDCT can aid in the early diagnosis of metastatic patients, inhibition of metastasis, and reduction of mortality.

Comparative analysis revealed that LRPAP1 was abundantly expressed in MIP (Fig. 4). LRPAP1 binds to and protects LRP1 as a chaperone protein and is essential for the absorption of low density and very low density lipoproteins into cells [17,53]. Here, each group was not significantly related to body mass index (Table S3). This suggests that LRPAP1 participates in MIP-mediated metastasis via a novel mechanism. Furthermore, we identified 30 proteins that were co-expressed with LRPAP1. All these proteins were highly expressed in tumors of the para-cancer samples from CPTAC (Fig. 5B). Consequently, LRPAP1 has an essential effect on tumors. Among those 30 co-expressed proteins, tumors were found to have high expression of the proteasome 26 S subunit, non-ATPase (PSMD) family proteins PSMD1 and PSMD3, and ATPase (PSMC) family proteins PSMC1 and PSMC4. The proteasome 26 S subunit, PSMD, and members of PSMC family participate in protein degradation, whereas PSMD1, PSMD3, PSMC1, and PSMC4 are linked to the progression of various tumors [54–57]. Heat shock protein 90 kDa alpha, class B, member 1 (HSP90AB1, called HSP90beta as well) was among those 30 co-expressed proteins and belonged to HSPs playing a role of molecular chaperones. It promotes tumorigenesis and tumor cell growth [58]. Our findings suggest that most proteins co-expressed with LRPAP1 play significant roles in tumors and that LRPAP1 probably has an important effect on MIP-associated metastasis.

In conclusion, LRPAP1 promoted tumor cell metastasis and invasion abilities and exhibited potent inhibition on tumor growth. However, further investigation is necessary to determine the mechanisms by which LRPAP1 promotes tumor metastasis. Our proteomic and experimental data revealed that LRPAP1 was highly expressed and promoted tumor cell metastasis in MIP. Taken together, our findings suggest LRPAP1 as a novel target for anti-metastatic therapy.

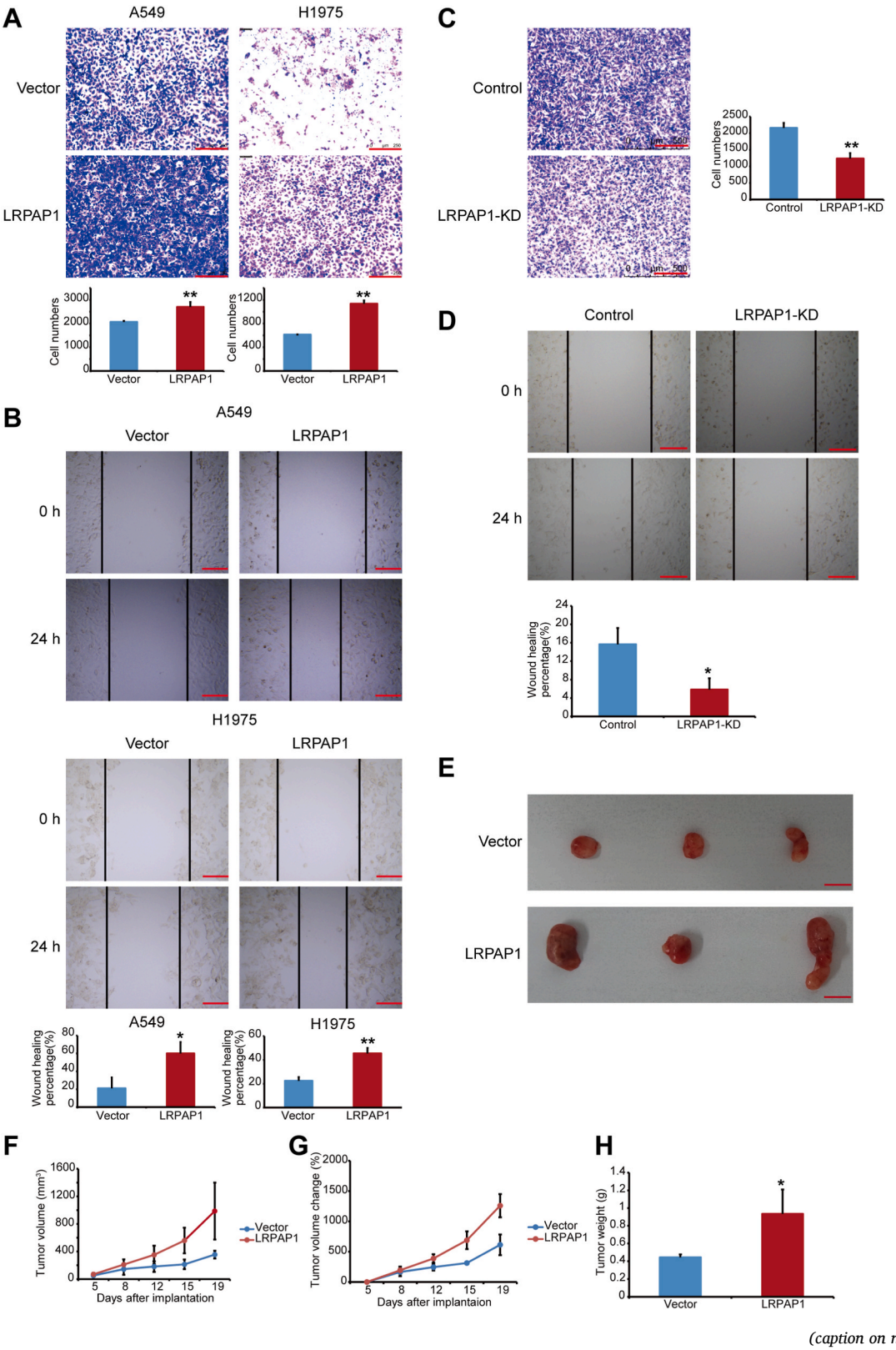

(caption on next page)

Fig. 6. LRPAP1 promotes cancer cell migration and metastasis. (A) Representative images (top, 24 h after seeding) and histograms (bottom) of the Transwell assay on A549 and H1975 cells overexpressing LRPAP1. (n = 3). Scale bar, 250 μm. (B) Typical images (top) and histograms (bottom) showing the wound-healing assay within A549 and H1975 cells with overexpressed LRPAP1. (n = 3). Scale bar, 150 μm. (C) Representative images (24 h after seeding) and corresponding histograms of the Transwell assay on A549 cells with knockdown of LRPAP1. (n = 3). Scale bar, 250 μm. (D) Representative images and corresponding histograms illustrating the wound-healing assay in A549 cells with knockdown of LRPAP1. (n = 3). Scale bar, 150 μm. (E) Subcutaneous injection of 5×10^6 cells into BALB/c nude mice led to tumor formation after a 19-day injection period (n = 3 per group). Scale bar, 1 cm. (F) Summary of tumor volume measurements obtained from mice. (G) Summary of tumor volume change in mice. (H) Histogram depicting the terminal weights of tumors. All data were presented as mean ± SD. Statistical significance between groups was determined using Student's t-test (*P < 0 0.05, **P < 0 0.01).

Ethics statement

This study was conducted according to the ethical principles of the Declaration of Helsinki. The present work gained approval from Cancer Hospital and Shenzhen Hospital, Chinese Academy of Medical Sciences and Peking Union Medical College Institutional Review Board of Clinical Research, (approval number: NO. KYKT2021-2-1). All participants provided informed consent to participate in the study. This work complied with all regulations.

All animal experimental protocols were approved by the Institutional Ethics Committees at Shenzhen People's Hospital (NO: AUP-220704-YHJ-0437-01). All animal experiments were conducted following the guidelines set by the Institutional Ethics Committees at Shenzhen People's Hospital. All methods are reported in accordance with ARRIVE guidelines.

Conflicts of interest/competing interests

The authors declare no conflicts of interest.

Funding statement

The present study was funded by the China Postdoctoral Science Foundation (2021M702290), Science and Technology Project of Shenzhen (No. GJHZ20170310090257380, JCYJ20170413092711058), Shenzhen Key Laboratory of Stem Cell Research and Clinical Transformation (ZDSYS20190902093203727), and National Natural Science Foundation of China (82001755).

Data availability statement

All data utilized in this work are publicly available from the ProteomeXchange Consortium (http://proteomecentral.proteomexchange.org) under the dataset identifier PXD038594.

CRediT authorship contribution statement

Hao-jie Yan: Writing – review & editing, Writing – original draft, Validation, Investigation, Funding acquisition, Data curation, Conceptualization. **Sheng-cheng Lin:** Writing – review & editing, Resources, Conceptualization. **Shao-hang Xu:** Data curation. **Yu-biao Gao:** Validation. **Bao-jin Zhou:** Data curation. **Ruo Zhou:** Data curation. **Fu-ming Chen:** Validation. **Fu-rong Li:** Writing – review & editing, Supervision, Funding acquisition, Conceptualization.

Declaration of competing interest

The authors declare that they have no known competing financial interests or personal relationships that could have appeared to influence the work reported in this paper.

Appendix A. Supplementary data

Supplementary data to this article can be found online at https://doi.org/10.1016/j.heliyon.2023.e23913.

References

[1] R.L. Siegel, et al., Cancer statistics, 2022, CA A Cancer J. Clin. 72 (1) (2022) 7–33.
[2] J. Ko, M.M. Winslow, J. Sage, Mechanisms of small cell lung cancer metastasis, EMBO Mol. Med. 13 (1) (2021), e13122.
[3] W.D. Travis, et al., International association for the study of lung cancer/american thoracic society/european respiratory society international multidisciplinary classification of lung adenocarcinoma, J. Thorac. Oncol. : Official Publication of the International Association For the Study of Lung Cancer 6 (2) (2011) 244–285.
[4] K.J. Butnor, Controversies and challenges in the histologic subtyping of lung adenocarcinoma, Transl. Lung Cancer Res. 9 (3) (2020) 839–846.

[5] E.E. Duhig, et al., Mitosis trumps T stage and proposed international association for the study of lung cancer/american thoracic society/european respiratory society classification for prognostic value in resected stage 1 lung adenocarcinoma, J. Thorac. Oncol. : Official Publication of the International Association For the Study of Lung Cancer 10 (4) (2015) 673–681.
[6] A. Warth, et al., The novel histologic International Association for the Study of Lung Cancer/American Thoracic Society/European Respiratory Society classification system of lung adenocarcinoma is a stage-independent predictor of survival, J. Clin. Oncol. : Official Journal of the American Society of Clinical Oncology 30 (13) (2012) 1438–1446.
[7] T.-E. Strand, et al., The percentage of lepidic growth is an independent prognostic factor in invasive adenocarcinoma of the lung, Diagn. Pathol. 10 (2015) 94.
[8] M. Kuang, et al., Clinical significance of complex glandular patterns in lung adenocarcinoma: clinicopathologic and molecular study in a large series of cases, Am. J. Clin. Pathol. 150 (1) (2018) 65–73.
[9] K. Kadota, et al., The cribriform pattern identifies a subset of acinar predominant tumors with poor prognosis in patients with stage I lung adenocarcinoma: a conceptual proposal to classify cribriform predominant tumors as a distinct histologic subtype, Mod. Pathol. : an Official Journal of the United States and Canadian Academy of Pathology, Inc 27 (5) (2014) 690–700.
[10] A. Warth, et al., Clinical relevance of different papillary growth patterns of pulmonary adenocarcinoma, Am. J. Surg. Pathol. 40 (6) (2016) 818–826.
[11] E. Thunnissen, et al., In compressed lung tissue microscopic sections of adenocarcinoma in situ may mimic papillary adenocarcinoma, Arch. Pathol. Lab Med. 137 (12) (2013) 1792–1797.
[12] A. Yoshizawa, et al., Validation of the IASLC/ATS/ERS lung adenocarcinoma classification for prognosis and association with EGFR and KRAS gene mutations: analysis of 440 Japanese patients, J. Thorac. Oncol. : Official Publication of the International Association For the Study of Lung Cancer 8 (1) (2013) 52–61.
[13] G. Lee, et al., Clinical impact of minimal micropapillary pattern in invasive lung adenocarcinoma: prognostic significance and survival outcomes, Am. J. Surg. Pathol. 39 (5) (2015) 660–666.
[14] C. Zhang, et al., Genomic landscape and immune microenvironment features of preinvasive and early invasive lung adenocarcinoma, J. Thorac. Oncol. 14 (11) (2019) 1912–1923.
[15] R. Caso, et al., The underlying tumor genomics of predominant histologic subtypes in lung adenocarcinoma, J. Thorac. Oncol. 15 (12) (2020) 1844–1856.
[16] J. Herz, et al., 39-kDa protein modulates binding of ligands to low density lipoprotein receptor-related protein/alpha 2-macroglobulin receptor, J. Biol. Chem. 266 (31) (1991) 21232–21238.
[17] T.E. Willnow, et al., Functional expression of low density lipoprotein receptor-related protein is controlled by receptor-associated protein in vivo, Proc. Natl. Acad. Sci. U.S.A. 92 (10) (1995) 4537–4541.
[18] M.A. Aldahmesh, et al., Mutations in LRPAP1 are associated with severe myopia in humans, Am. J. Hum. Genet. 93 (2) (2013) 313–320.
[19] A.O. Khan, M.A. Aldahmesh, F.S. Alkuraya, Clinical characterization of LRPAP1-related pediatric high myopia, Ophthalmology 123 (2) (2016) 434–435.
[20] L. Thurner, et al., LRPAP1 is a frequent proliferation-inducing antigen of BCRs of mantle cell lymphomas and can be used for specific therapeutic targeting, Leukemia 33 (1) (2019) 148–158.
[21] L. Thurner, et al., LRPAP1 autoantibodies in mantle cell lymphoma are associated with superior outcome, Blood 137 (23) (2021) 3251–3258.
[22] M. Sumazaki, et al., Serum anti-LRPAP1 is a common biomarker for digestive organ cancers and atherosclerotic diseases, Cancer Sci. 111 (12) (2020) 4453–4464.
[23] F. Coscia, et al., A streamlined mass spectrometry-based proteomics workflow for large-scale FFPE tissue analysis, J. Pathol. 251 (1) (2020) 100–112.
[24] J.R. Wiśniewski, et al., Universal sample preparation method for proteome analysis, Nat. Methods 6 (5) (2009) 359–362.
[25] V. Demichev, et al., DIA-NN: neural networks and interference correction enable deep proteome coverage in high throughput, Nat. Methods 17 (1) (2020) 41–44.
[26] L. Shao, et al., MicroRNA-326 attenuates immune escape and prevents metastasis in lung adenocarcinoma by targeting PD-L1 and B7-H3, Cell Death Dis. 7 (1) (2021) 145.
[27] H.T. Luo, et al., Dissecting the multi-omics atlas of the exosomes released by human lung adenocarcinoma stem-like cells, NPJ Genom Med 6 (1) (2021) 48.
[28] Y. Wang, et al., ASPP2 controls epithelial plasticity and inhibits metastasis through β-catenin-dependent regulation of ZEB1, Nat. Cell Biol. 16 (11) (2014) 1092–1104.
[29] J. Pan, et al., Qingfei Jiedu decoction inhibits PD-L1 expression in lung adenocarcinoma based on network pharmacology analysis, molecular docking and experimental verification, Front. Pharmacol. 13 (2022).
[30] J. Ma, et al., iProX: an integrated proteome resource, Nucleic Acids Res. 47 (D1) (2019) D1211–D1217.
[31] T. Chen, et al., iProX in 2021: connecting proteomics data sharing with big data, Nucleic Acids Res. 50 (D1) (2022) D1522–D1527.
[32] J.L. Hopkins, L. Lan, L. Zou, DNA repair defects in cancer and therapeutic opportunities, Gene Dev. 36 (5–6) (2022) 278–293.
[33] J.M. Cleary, et al., Biomarker-guided development of DNA repair inhibitors, Mol. Cell 78 (6) (2020) 1070–1085.
[34] P.A. Jeggo, L.H. Pearl, A.M. Carr, DNA repair, genome stability and cancer: a historical perspective, Nat. Rev. Cancer 16 (1) (2016) 35–42.
[35] B. Vogelstein, D. Lane, A.J. Levine, Surfing the p53 network, Nature 408 (6810) (2000) 307–310.
[36] Z. Wang, A. Strasser, G.L. Kelly, Should mutant TP53 be targeted for cancer therapy? Cell Death Differ. 29 (5) (2022) 911–920.
[37] Y.-H. Wang, et al., Rapid recruitment of p53 to DNA damage sites directs DNA repair choice and integrity, Proc. Natl. Acad. Sci. U.S.A. 119 (10) (2022), e2113233119.
[38] M.R. Clarke, et al., Extracellular matrix expression in metastasizing and nonmetastasizing adenocarcinomas of the lung, Hum. Pathol. 28 (1) (1997) 54–59.
[39] S.R. Polio, et al., Extracellular matrix stiffness regulates human airway smooth muscle contraction by altering the cell-cell coupling, Sci. Rep. 9 (1) (2019) 9564.
[40] D. Tewari, et al., Natural products targeting the PI3K-Akt-mTOR signaling pathway in cancer: a novel therapeutic strategy, Semin. Cancer Biol. 80 (2022).
[41] M.K. Edirisweera, K.H. Tennekoon, S.R. Samarakoon, Role of the PI3K/AKT/mTOR signaling pathway in ovarian cancer: biological and therapeutic significance, Semin. Cancer Biol. 59 (2019) 147–160.
[42] A.S. Alzahrani, PI3K/Akt/mTOR inhibitors in cancer: at the bench and bedside, Semin. Cancer Biol. 59 (2019) 125–132.
[43] A. Maynard, et al., Therapy-Induced evolution of human lung cancer revealed by single-cell RNA sequencing, Cell 182 (5) (2020).
[44] Y. Xue, et al., Evolution from genetics to phenotype: reinterpretation of NSCLC plasticity, heterogeneity, and drug resistance, Protein & Cell 8 (3) (2017) 178–190.
[45] B. Hwang, J.H. Lee, D. Bang, Single-cell RNA sequencing technologies and bioinformatics pipelines, Exp. Mol. Med. 50 (8) (2018).
[46] M. Karlsson, et al., A single-cell type transcriptomics map of human tissues, Sci. Adv. 7 (31) (2021).
[47] C.E. Barkauskas, et al., Lung organoids: current uses and future promise, Development (Cambridge, U. K.) 144 (6) (2017) 986–997.
[48] L. Cassetta, J.W. Pollard, Targeting macrophages: therapeutic approaches in cancer, Nat. Rev. Drug Discov. 17 (12) (2018) 887–904.
[49] Y. Xia, et al., Engineering macrophages for cancer immunotherapy and drug delivery, Adv. Mater. 32 (40) (2020), e2002054.
[50] Y.J. Chen, et al., Proteogenomics of non-smoking lung cancer in east asia delineates molecular signatures of pathogenesis and progression, Cell 182 (1) (2020) 226–244.e17.
[51] J.L. Dickson, et al., Hesitancy around low-dose CT screening for lung cancer, Ann. Oncol. : Official Journal of the European Society For Medical Oncology 33 (1) (2022) 34–41.
[52] X. Hua, et al., Targeting USP22 with miR-30-5p to inhibit the hypoxia-induced expression of PD-L1 in lung adenocarcinoma cells, Oncol. Rep. 46 (4) (2021).
[53] T.E. Willnow, et al., RAP, a specialized chaperone, prevents ligand-induced ER retention and degradation of LDL receptor-related endocytic receptors, EMBO J. 15 (11) (1996) 2632–2639.
[54] A.J. Rubio, et al., 26S proteasome non-ATPase regulatory subunits 1 (PSMD1) and 3 (PSMD3) as putative targets for cancer prognosis and therapy, Cells 10 (9) (2021).
[55] L. Liu, et al., Proteasome 26S subunit, non-ATPase 1 (PSMD1) facilitated the progression of lung adenocarcinoma by the de-ubiquitination and stability of PTEN-induced kinase 1 (PINK1), Exp. Cell Res. 413 (2) (2022), 113075.

[56] A. Salah Fararjeh, et al., The prognostic significance of proteasome 26S subunit, non-ATPase (PSMD) genes for bladder urothelial carcinoma patients, Cancer Inf. 20 (2021), 11769351211067692.
[57] T.J. Kao, et al., Prognoses and genomic analyses of proteasome 26S subunit, ATPase (PSMC) family genes in clinical breast cancer, Aging (Albany NY) 13 (14) (2021), 17970.
[58] M. Haase, G. Fitze, HSP90AB1: helping the good and the bad, Gene 575 (2 Pt 1) (2016) 171–186.